applied sciences

MDPI

Article

Yield Behaviour of Welded I-Shaped Steel Cross-Sections

Luigi Palizzolo and Salvatore Benfratello *

Department of Engineering, University of Palermo, Viale delle Scienze, I-90128 Palermo, Italy; luigi.palizzolo@unipa.it
* Correspondence: salvatore.benfratello@unipa.it

Abstract: The limit behaviour of I-shaped welded steel cross-sections subjected to axial force, shear, and bending moment is a crucial matter to ascertain the reliability of framed structures constituted by non-standard beam elements. International standards provide an approximate solution to the problem, and other studies have proposed improved approximate formulations to ascertain the real features of the relevant cross-sections. The present paper is devoted to enhancing the problem of the limit behaviour of plane I-shaped welded steel cross-sections subjected to axial force (N), shear (T) and bending moment (M); therefore, new appropriate formulations are proposed in order to define suitable new domains, both in planes (N,T), (N,M), and (M,T) and in the space (N,T,M). The material is assumed as elastic–perfectly plastic and the Von Mises limit condition is adopted as the resistance criterion. The elastic stresses are described by the Navier formula and the Jourawski formula. The limit stress condition related to the contemporaneous presence of the acting forces is defined as the one that, at each point of the cross-section, fulfils the Von Mises limit condition as equality. The formulation is rigorously devoted to factory-made welded I-shaped steel cross-sections. Some numerical examples are reported in the application stage and useful comparison are carried out, with the results being obtainable by the application of the classical known standard formulae, proving the reliability and effectiveness of the determined domains.

Keywords: welded sections; steel; plane stresses; yield domains; international standards

Citation: Palizzolo, L.; Benfratello, S. Yield Behaviour of Welded I-Shaped Steel Cross-Sections. *Appl. Sci.* **2024**, *14*, 8037. https://doi.org/10.3390/app14178037

Academic Editors: Ana Pavlovic and Ivana D. Atanasovska

Received: 5 August 2024
Revised: 27 August 2024
Accepted: 6 September 2024
Published: 8 September 2024

1. Introduction

In many cases of practical interest, in the design of steel frame structures, it is very useful to adopt factory-welded I-shaped beams instead of the standard rolled ones. One of these cases is that of seismic retrofitting of existing masonry structures. In such a case, to obtain the required seismic behaviour, it is necessary to modify the stiffness of the masonry panels. For this goal, steel hooping is considered the most adequate, and the adoption of suitably designed and factory-welded steel elements allows us to obtain optimal structures with reduced size and, consequently, with little effect on usability. Another task is that of new openings in masonry panels, which requires the steel hooping to restore both strength and stiffness of those panels where the opening is created. In such cases, usually, the required stiffness is often very high and, consequently, the chance of adopting steel frames realized with suitably designed and factory-welded I-shaped beam elements with assigned geometric characteristics is a fundamental strategy which also allows for a reduction in the opening dimensions.

On the other hand, the above referenced chance of adopting welded structural elements is also often advantageous in new frame design. As is well known in such structures, the connections between beams and columns are very critical, since their design plays a crucial role in the safety and ductility of the overall structure. This topic is relevant when elastoplastic analysis is performed both statically [1–4] or dynamically [5–9], as well as in design problems for frame and truss structures [10–12], both taking into account buckling and slenderness [13–16] and in the case of seismic and dynamic actions [17–20].

In practical applications, an important strategy is to plan interventions able to reduce the strength of the element in suitably selected portions of the element close to the connec-

tions between beams and columns. In this way, the onset of plastic strain also allows for the protection of the welded connections between beams and columns. The most common approach belonging to this strategy is the so-called dogbone, while a recently proposed approach is referred to as the Limited Resistance Plastic Device (LRPD). Another approach is based on dissipative approaches leading, e.g., to devices for seismic-resistant steel frames developed by the FUSEIS EC project (RFSR-CT-2008-00032) or other devices [21–24].

The main idea of the dogbone [25–29] is that of suitably reducing the base of the I-shaped beam in a portion close to the column to obtain a reduction in the limit bending moment. Such a reduction in the case of high loads causes the required yielding and decreases in the actions on the welded connections between beams and columns. The seismic performances of structures equipped with dogbones is the topic of many papers available in the literature (see, e.g., [30–32]), and developments of the main idea (i.e., reducing the web) have been also proposed (see, e.g., [33–36]).

In recent years, a number of innovative systems based on energy dissipation and damping have been invented as a result of national and European research projects, such as dissipative connections assigned to braced steel frames (developed in "Two INnovations for Earthquake Resistant Design", INERD project) [24] and dissipative links (see, e.g., [37,38]). These innovative systems consist of small and dismountable dissipative parts where seismic damage is concentrated; hence, they have increased repairability while displaying comparable stiffness and ductility to the conventional ones. The structural behaviour of structures equipped with these devices is assessed in many papers available in the literature (see, e.g., [39]).

The LRPDs represent the most recent proposal in this topic; these innovative devices can be positioned either at the ends of beams and at the bases of columns, and their peculiar design not only incites the onset of plastic strains on the selected portions of the equipped beam elements, but, furthermore, also guarantees the invariance of the bending stiffness of the overall involved elements.

The first version of LRPD was referred to as limited-resistance rigid perfectly plastic flexural hinges (LRPH). Later, the design problem was enriched by taking into account the simultaneous presence of both normal and tangential stresses and adopting a special analysis of the beam elements by means of smart beam elements specialized to the design of a frame with assigned capacity curve [40], as well as performing both numerical and experimental validation. Other formulations, among which one is approximated to be useful in practical applications, have been proposed to compare the results with those achieved by different typologies of reduced beam section (RBS) connections [41]; some new formulations have also been proposed to consider the local buckling and to protect the welded connections between beams and columns [42].

The actual version, referred to as LRPD, is a beam element with multistep geometry, constituted by three subsequent I-shaped portions whose web and flange thicknesses are suitably designed.

In this last version of LRPD, the inner portion with reduced dimensions shows limited strength and allows the onset of plastic strain, while the outer portions are equal to each other and show greater web and flange thicknesses to guarantee that the bending stiffness of the overall involved element is unaltered. As can be easily deduced, the LRPD design requires the solution to appropriate optimal design problems, and their production has to be performed in a factory by welding steel plates of appropriate thickness.

Expanding the focus to welded I-shaped sections of any size and referring to beam elements belonging to frame structures, these sections are subjected to the simultaneous action of axial force N, shear force T, and bending moment M. It is evident that the knowledge of both the elastic and plastic limit domains of such sections is essential to evaluate the overall structural safety. The actual international standards [43] provide approximated expressions to identify such domains, and, therefore, it is appropriate to examine this topic in depth to obtain more rigorous expressions for practical applications. In the literature, some papers have recently been proposed for either elastic [41] or plastic [44],

domains but the formulations for plastic domains still present approximations, and they involve standard sections.

Therefore, the aim of the present paper is to propose a rigorous procedure to identify the plastic domains of welded I-shaped sections subjected to the simultaneous action of axial force N, shear force T, and bending moment M, assuming an elastic–perfectly plastic material behaviour and imposing that the section belongs to Class 1 of the EC3 standard [43]. The expressions of the plastic domain contours in the $(N, T,\ M)$ space, as well as those in the (N, M), (N, T), and (M, T) planes, will be provided. Some numerical applications for the case of welded sections and a comparison with the results from the EC3 standard conclude the paper.

2. Materials and Methods

The mechanical behaviour of the I-shaped welded section sketched in Figure 1, subjected to the simultaneous presence of axial force N, shear force T_z, and bending moment M_y, is presented. An elastic–perfectly plastic behaviour of the material is considered, and the adopted yielding criterion is the Von Mises one:

$$\sigma_0^2 = \sigma_x^2 + 3\left(\tau_{xy}^2 + \tau_{xz}^2\right) \tag{1}$$

σ_0 is the yielding stress of the material. Due to the symmetry of the domains to be determined with respect to the (N, M), (N, T), (T, M) planes as well as in the space (N, T, M), in the following section, reference will be made only to positive quadrants or octants.

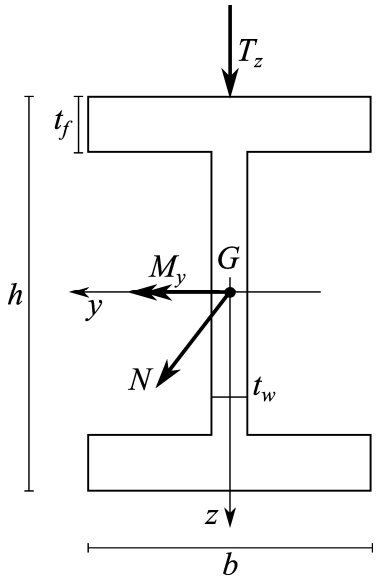

Figure 1. Geometrical sketch of the cross-section with the acting internal forces.

Referring to the geometrical characteristics of the section reported in Appendix A, the following limit internal forces can be determined:

$$N_E = \ N_p = A\sigma_0 \tag{2}$$

$$M_E = W_{Ey}\sigma_0 \tag{3}$$

$$M_p = W_{py}\sigma_0 \tag{4}$$

$$T_E = \frac{\sigma_0}{\sqrt{3}} \frac{I_y t_w}{S_{y,G}} \tag{5}$$

$$T_p = \frac{\sigma_0}{\sqrt{3}} t_w \left(h - 2t_f\right) + 2 \frac{\sigma_0 t_w}{\sqrt{3} \cdot S_y\left(\frac{h}{2} - t_f\right)} \int_{\frac{h}{2}-t_f}^{\frac{h}{2}} S_y(z) dz \tag{6}$$

N_E, N_p, M_E, M_p, T_E, and T_p are the elastic and plastic limit axial force, bending moment, and shear force, respectively. In Equation (5), $\tau_0 = \sigma_0/\sqrt{3}$ is assumed. In Equation (6) T_p is derived referring to the limit condition sketched in Figure 2, that is, the web is assumed to be fully plasticized and the presence of τ_{xz} in the flanges is taken into account.

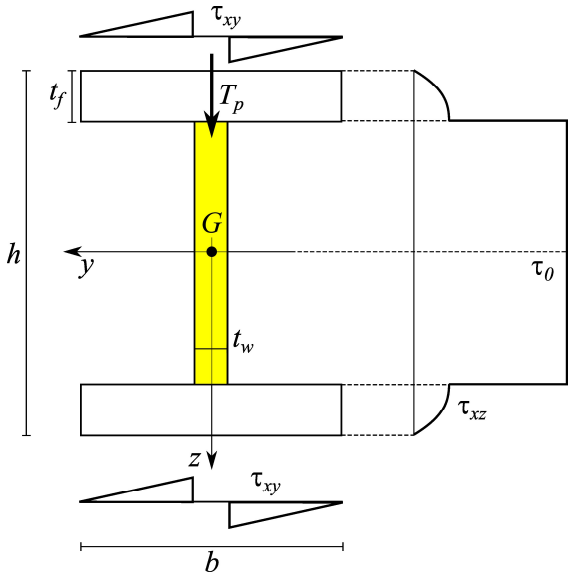

Figure 2. Tangential stress (τ_{xy}, τ_{xz}) diagrams for $T = T_p$.

The following final remarks can be made: when $N = N_p$, then $T = 0$ and $M = 0$ result; when $M = M_p$, then $N = 0$ and $T = 0$ result; when $T = T_p$, then $N \neq 0$ and $M \neq 0$ can be.

2.1. Simultaneous Presence of $T = T_p$ and N ($M = 0$)

The presence of T_p as the acting shear force does not exclude the simultaneous presence of a limited axial force. In such a case, all along the web, $\tau_{xz} = \tau_0 = \sigma_0/\sqrt{3}$ occurs, so the presence of normal stresses is excluded. Instead, in the flanges, both τ_{xy} and τ_{xz} are present, assuming values lesser than τ_0, so that the presence of normal stresses is possible. Referring to Figure 3a, in the ranges $\frac{h}{2} - t_f \leq z \leq \frac{h}{2}$ and $\frac{t_w}{2} \leq y \leq \frac{b}{2}$, the expression of τ_{xy} is given by the following relation:

$$\left|\tau_{xy}(y)\right| = \frac{T_p\left(\frac{b}{2} - y\right)\left(h - t_f\right)}{2I_y} \tag{7}$$

The expression of τ_{xz}, in the ranges $\frac{h}{2} - t_f \leq z \leq \frac{h}{2}$ and $0 \leq y \leq \frac{b}{2}$ (Figure 3b), is given by:

$$\left|\tau_{xz}(z)\right| = \frac{T_p\left(\frac{h^2}{4} - z^2\right)}{2I_y} \tag{8}$$

By imposing the full yielding condition on all the points of the cross-section in the ranges $\frac{h}{2} - t_f \leq z \leq \frac{h}{2}$ and $\frac{t_w}{2} \leq y \leq \frac{b}{2}$, the normal stresses acting in the flange must respect Equation (1) as equality; that is, taking into account Equations (1), (7), and (8), the following relation is obtained:

$$\sigma_x(y,z) = \sqrt{\sigma_0^2 - 3\frac{T_p^2}{4I_y^2}\left[\left(\frac{b}{2} - y\right)^2\left(h - t_f\right)^2 + \left(\frac{h^2}{4} - z^2\right)^2\right]} \tag{9}$$

By imposing the full yielding condition on all the points of the cross-section where $\tau_{xy} = 0$ (i.e., in the ranges $\frac{h}{2} - t_f \leq z \leq \frac{h}{2}$ and $0 \leq y \leq \frac{t_w}{2}$), the normal stresses acting in the flange must respect Equation (1) as equality; that is, taking into account Equations (1) and (8), the following relation is obtained:

$$\sigma_x(z) = \sqrt{\sigma_0^2 - 3\frac{T_p^2\left(\frac{h^2}{4} - z^2\right)^2}{4I_y^2}} \tag{10}$$

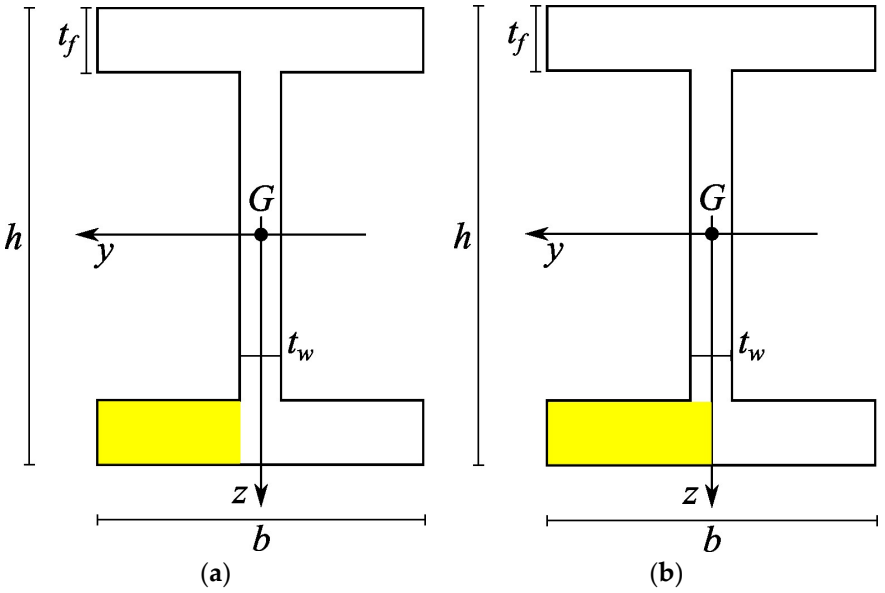

Figure 3. Portion of the cross-section considered: (**a**) in Equation (7); (**b**) in Equation (8).

It follows that the limit axial force acting when $T = T_p$ is given by:

$$\begin{aligned} N_{\ell im}(T_p) = 4\int_{\frac{t_w}{2}}^{\frac{b}{2}}\left[\int_{\frac{h}{2}-t_f}^{\frac{h}{2}}\sqrt{\sigma_0^2 - 3\frac{T_p^2}{4I_y^2}\left[\left(\frac{b}{2} - y\right)^2\left(h - t_f\right)^2 + \left(\frac{h^2}{4} - z^2\right)^2\right]}dz\right]dy \\ +2t_w\int_{\frac{h}{2}-t_f}^{\frac{h}{2}}\sqrt{\sigma_0^2 - 3\frac{T^2\left(\frac{h^2}{4} - z^2\right)^2}{4I_y^2}}dz \end{aligned} \tag{11}$$

The pair of values $N_{\ell im}(T_p), T_p$ represents the internal force condition, which determines the full yielding of the whole cross-section. It is worth noting that all the pairs of values $N,\ T_p$, with $0 \leq N < N_{\ell im}(T_p)$, always represent limit conditions, but only for shear; indeed, in this latter condition, the shear force reaches its limit yield value, but the

web suffers plastic strains due to the shear, while the flanges behave elastically. It follows that the segment $\left[0, T_p; N_{\ell im}(T_p), T_p\right]$ in the plane N, T represents the upper plateau of the relevant yield domain boundary. The entire yield domain boundary is defined in Section 2.4 and is represented in the application stage for two representative cross-sections.

2.2. Simultaneous Presence of $T = T_p$ and M $(N = 0)$

Analogously, on the grounds of Equations (7)–(10), the limit bending moment acting when $T = T_p$ is given by:

$$M_{\ell im}(T_p) = 4\int_{\frac{t_w}{2}}^{\frac{b}{2}}\left[\int_{\frac{h}{2}-t_f}^{\frac{h}{2}}\sqrt{\sigma_0^2 - 3\frac{T_p^2}{4I_y^2}\left[\left(\frac{b}{2}-y\right)^2\left(h-t_f\right)^2 + \left(\frac{h^2}{4}-z^2\right)^2\right]}\,z\,dz\right]dy + 2t_w\int_{\frac{h}{2}-t_f}^{\frac{h}{2}}\sqrt{\sigma_0^2 - 3\frac{T^2\left(\frac{h^2}{4}-z^2\right)^2}{4I_y^2}}\,z\,dz \tag{12}$$

As previously noted for the axial force, the pair of values $M_{\ell im}(T_p), T_p$ represents the internal force condition, which determines the full yielding of the whole cross-section. It is worth noting that all the pairs of values M, T_p, with $0 \leq M < M_{\ell im}(T_p)$, always represent limit conditions, but only for shear; indeed, in the latter condition, the shear force reaches its limit yield value, but the web suffers plastic strains due to the shear, while the flanges behave elastically. It follows that the segment $\left[0, T_p; M_{\ell im}(T_p), T_p\right]$ in the plane M, T represents the upper plateau of the relevant yield domain boundary. The entire yield domain boundary is defined in Section 2.5 and represented in the application stage for two representative cross-sections.

2.3. Simultaneous Presence of $T = T_p$ N and M

A successive step is considering the simultaneous presence of T_p as the acting shear force together with both the axial force $N < N_{\ell im}(T_p)$ and bending moment $M < M_{\ell im}(T_p)$.

With the aim of taking into account the influence of both the axial force and bending moment, reference can be made to the usual procedure utilized for the definition of the yield domain in the plane N, M. Therefore, each flange is divided in two parts by a segment parallel to the y-axis; the inner ones are subjected to normal stress related to the axial force, while the outer ones to normal stresses related to the bending moment. Due to these remarks, the distance $z = z_N$ dividing the above-described parts lies in the range $\frac{h}{2} - t_f \leq z_N \leq \frac{h}{2}$. The infinite pairs of N, M values which determine the yielding conditions for the whole cross-section are given by the following relations:

$$N(T_p) = 4\int_{\frac{t_w}{2}}^{\frac{b}{2}}\left[\int_{\frac{h}{2}-t_f}^{z_N}\sqrt{\sigma_0^2 - 3\frac{T_p^2}{4I_y^2}\left[\left(\frac{b}{2}-y\right)^2\left(h-t_f\right)^2 + \left(\frac{h^2}{4}-z^2\right)^2\right]}\,dz\right]dy + 2t_w\int_{\frac{h}{2}-t_f}^{z_N}\sqrt{\sigma_0^2 - 3\frac{T_p^2\left(\frac{h^2}{4}-z^2\right)^2}{4I_y^2}}\,dz \tag{13}$$

$$M(T_p) = 4\int_{\frac{t_w}{2}}^{\frac{b}{2}}\left[\int_{z_N}^{\frac{h}{2}}\sqrt{\sigma_0^2 - 3\frac{T_p^2}{4I_y^2}\left[\left(\frac{b}{2}-y\right)^2\left(h-t_f\right)^2 + \left(\frac{h^2}{4}-z^2\right)^2\right]}zdz\right]dy + 2t_w\int_{z_N}^{\frac{h}{2}}\sqrt{\sigma_0^2 - 3\frac{T_p^2\left(\frac{h^2}{4}-z^2\right)^2}{4I_y^2}}zdz \tag{14}$$

It is worth noting that the deduced values define a plane boundary for $T = T_p$; the surface within this boundary is the locus of the points for which the yield condition is reached referring just the shear force, while the flanges still behave in an elastic condition.

2.4. Yield Domain in N, T Plane ($M = 0$)

The next step is to define the boundary of the yield domain N, T. To this goal the range $0 \le T \le T_P$ is divided in the following subranges $0 \le T \le T_E$ and $T_E \le T \le T_p$.

In the range $0 \le T \le T_E$, for an assigned value of the shear force T, the expression of τ_{xy}, for $\frac{h}{2} - t_f \le z \le \frac{h}{2}$ and $\frac{t_w}{2} \le y \le \frac{b}{2}$, is given by:

$$\left|\tau_{xy}(y)\right| = \frac{T\left(\frac{b}{2}-y\right)\left(h-t_f\right)}{2I_y} \tag{15}$$

In the flange identified by the ranges $\frac{h}{2} - t_f \le z \le \frac{h}{2}$ and $0 \le y \le \frac{b}{2}$, the expression of τ_{xz} is given by:

$$|\tau_{xz}(z)| = \frac{T\left(\frac{h^2}{4}-z^2\right)}{2I_y} \tag{16}$$

In the web, for the range $0 \le z \le \frac{h}{2} - t_f$, τ_{xz} is given by:

$$|\tau_{xz}(z)| = \frac{T\left\{bt_f\left(h-t_f\right) + t_w\left[\left(\frac{h}{2}-t_f\right)^2 - z^2\right]\right\}}{2I_y t_w} \tag{17}$$

By imposing the Von Mises full yielding condition in all points of the cross-section where both tangential stresses are present, the following expression for $\sigma_x(y,z)$ is obtained:

$$\sigma_x(y,z) = \sqrt{\sigma_0^2 - 3\frac{T^2}{4I_y^2}\left[\left(\frac{b}{2}-y\right)^2\left(h-t_f\right)^2 + \left(\frac{h^2}{4}-z^2\right)^2\right]} \tag{18}$$

By performing analogous steps for the flange portion where only $\tau_{xz}(z)$ acts, the following relation is obtained:

$$\sigma_x(z) = \sqrt{\sigma_0^2 - 3\frac{T^2\left(\frac{h^2}{4}-z^2\right)^2}{4I_y^2}} \tag{19}$$

By performing analogous steps for the web where only $\tau_{xz}(z)$ acts, the following relation is obtained:

$$\sigma_x(z) = \sigma_x(z) = \sqrt{\sigma_0^2 - 3\frac{T^2\left\{bt_f\left(h-t_f\right) + t_w\left[\left(\frac{h}{2}-t_f\right)^2 - z^2\right]\right\}^2}{4I_y^2 t_w^2}} \tag{20}$$

Finally, the limit axial force $N_{\ell im}(T)$ is given by

$$N_{\ell im}(T) = 4\int_{\frac{t_w}{2}}^{\frac{b}{2}}\left[\int_{\frac{h}{2}-t_f}^{\frac{h}{2}}\sqrt{\sigma_0^2 - 3\frac{T^2}{4I_y^2}\left[\left(\frac{b}{2}-y\right)^2\left(h-t_f\right)^2 + \left(\frac{h^2}{4}-z^2\right)^2\right]}dz\right]dy$$
$$+2t_w\int_{\frac{h}{2}-t_f}^{\frac{h}{2}}\sqrt{\sigma_0^2 - 3\frac{T^2\left(\frac{h^2}{4}-z^2\right)^2}{4I_y^2}}dz \tag{21}$$
$$+2t_w\int_{0}^{\frac{h}{2}-t_f}\sqrt{\sigma_0^2 - 3\frac{T^2\left\{bt_f\left(h-t_f\right) + t_w\left[\left(\frac{h}{2}-t_f\right)^2 - z^2\right]\right\}^2}{4I_y^2t_w^2}}dz$$

In the range $T_E \le T \le T_P$ a portion of the web is fully plasticized with $\tau_{xz} = \tau_0 = \sigma_0/\sqrt{3}$ due to the acting shear. In the other portions of the web, τ_{xz} shows the usual parabolic expression, while in the flanges, τ_{xy} acts with a linear expression.

Let the fully plasticized portion of the web be identified by a value of $z = \overline{z}$ in the range of $\left(0,\ \frac{h}{2} - t_f\right)$. Clearly, in this portion:

$$\tau_{xz}(\overline{z}) = \frac{\sigma_0}{\sqrt{3}} \tag{22}$$

In the remaining portion of the web, i.e., for $\overline{z} \le z \le \frac{h}{2} - t_f$,

$$\tau_{xz}(z) = \frac{\sigma_0}{\sqrt{3}}\frac{S_y(z)}{S_y(\overline{z})} \tag{23}$$

In the flanges, for $\frac{h}{2} - t_f \le z \le \frac{h}{2}$,

$$\tau_{xz}(z) = \frac{\sigma_0}{\sqrt{3}}\frac{S_y(z)}{S_y(\overline{z})}\frac{t_w}{b} \tag{24}$$

It follows that, for an assigned $0 \le \overline{z} \le \frac{h}{2} - t_f$, the shear force is given by:

$$T(\overline{z}) = \frac{\sigma_0}{\sqrt{3}}2t_w\overline{z} + 2\int_{\overline{z}}^{\frac{h}{2}-t_f}\frac{\sigma_0}{\sqrt{3}}\frac{S_y(z)}{S_y(\overline{z})}t_w dz + 2\int_{\frac{h}{2}-t_f}^{\frac{h}{2}}\frac{\sigma_0}{\sqrt{3}}\frac{S_y(z)}{S_y(\overline{z})}t_w dz \tag{25}$$

In the web portion outside the fully plasticized one, the acting normal stress must fulfil the Von Mises yielding condition, leading to the following relation:

$$\sigma_x(z) = \sigma_x(z) = \sigma_0\sqrt{1 - \left[\frac{S_y(z)}{S_y(\overline{z})}\right]^2} \tag{26}$$

and, as a consequence, the axial force $N_{\ell im}[T(\overline{z})]$ reads

$$N_{\ell im}[T(\bar{z})] = 4\int_{\frac{t_w}{2}}^{\frac{b}{2}}\left[\int_{\frac{h}{2}-t_f}^{\frac{h}{2}}\sqrt{\sigma_0^2 - 3\frac{T^2(\bar{z})}{4I_y^2}\left[\left(\frac{b}{2}-y\right)^2\left(h-t_f\right)^2 + \left(\frac{h^2}{4}-z^2\right)^2\right]}dz\right]dy$$
$$+2t_w\int_{\frac{h}{2}-t_f}^{\frac{h}{2}}\sqrt{\sigma_0^2 - 3\frac{T^2(\bar{z})\left(\frac{h^2}{4}-z^2\right)^2}{4I_y^2}}dz \quad (27)$$
$$+2t_w\int_{\bar{z}}^{\frac{h}{2}-t_f}\sqrt{\sigma_0^2 - 3\frac{T^2(\bar{z})\left\{bt_f\left(h-t_f\right)+t_w\left[\left(\frac{h}{2}-t_f\right)^2 - z^2\right]\right\}^2}{4I_y^2t_w^2}}dz$$

2.5. Yield Domain in M, T Plane $(N = 0)$

The boundary of the yield domain in the plane M, T can be defined by performing analogous steps to those in the foregoing section. Therefore, the following relations are obtained.

In the range $0 \le T \le T_E$, $M_{\ell im}(T)$ is given by:

$$M_{\ell im}(T) = 4\int_{\frac{t_w}{2}}^{\frac{b}{2}}\left[\int_{\frac{h}{2}-t_f}^{\frac{h}{2}}\sqrt{\sigma_0^2 - 3\frac{T^2}{4I_y^2}\left[\left(\frac{b}{2}-y\right)^2\left(h-t_f\right)^2 + \left(\frac{h^2}{4}-z^2\right)^2\right]}zdz\right]dy$$
$$+2t_w\int_{\frac{h}{2}-t_f}^{\frac{h}{2}}\sqrt{\sigma_0^2 - 3\frac{T^2\left(\frac{h^2}{4}-z^2\right)^2}{4I_y^2}}zdz \quad (28)$$
$$+2t_w\int_{0}^{\frac{h}{2}-t_f}\sqrt{\sigma_0^2 - 3\frac{T^2\left\{bt_f\left(h-t_f\right)+t_w\left[\left(\frac{h}{2}-t_f\right)^2 - z^2\right]\right\}^2}{4I_y^2t_w^2}}zdz$$

In the range $T_E \le T \le T_p$, $M_{\ell im}(T)$ is given by:

$$M_{\ell im}[T(\bar{z})] = 4\int_{\frac{t_w}{2}}^{\frac{b}{2}}\left[\int_{\frac{h}{2}-t_f}^{\frac{h}{2}}\sqrt{\sigma_0^2 - 3\frac{T^2(\bar{z})}{4I_y^2}\left[\left(\frac{b}{2}-y\right)^2\left(h-t_f\right)^2 + \left(\frac{h^2}{4}-z^2\right)^2\right]}zdz\right]dy$$
$$+2t_w\int_{\frac{h}{2}-t_f}^{\frac{h}{2}}\sqrt{\sigma_0^2 - 3\frac{T^2(\bar{z})\left(\frac{h^2}{4}-z^2\right)^2}{4I_y^2}}zdz \quad (29)$$
$$+2t_w\int_{\bar{z}}^{\frac{h}{2}-t_f}\sigma_0\sqrt{\sigma_0^2 - 3\frac{T^2(\bar{z})\left\{bt_f\left(h-t_f\right)+t_w\left[\left(\frac{h}{2}-t_f\right)^2 - z^2\right]\right\}^2}{4I_y^2t_w^2}}zdz$$

2.6. Yield Domain in N, T, M Space

For $T = T_p$, the yield conditions for N and M have been already determined in the foregoing sections by Equations (13) and (14). In the following section, the relations characterizing the 3D domain N, T, M will be determined separately by considering the two subsequent ranges: $0 \leq T \leq T_E$ and $T_E \leq T \leq T_p$.

In the range $0 \leq T \leq T_E$, the 3D domain N, T, M is obtained by assigning a set of values to T and determining the consequent N, M plane domain boundaries. To this aim, as usual, increasing values to z_N are assigned, with $0 \leq z_N \leq \frac{h}{2}$, $2z_N$ being the portion of the cross-section area (symmetric with respect to the y-axis) that reaches the full plasticization as a result of the presence of shear force and axial force. For the typical value of T, in the flanges, τ_{xy} shows the expression reported in Equation (15), while τ_{xz} shows the expression reported in Equation (16). In the web, the expression of τ_{xz} shows the expression reported in Equation (17). It is important to note that, due to the geometric discontinuities characterizing the shape of the section under consideration for $z_N = \frac{h}{2} - t_f$, the relations which define the limit values for N and M are defined for each range: $0 \leq z_N \leq \frac{h}{2} - t_f$ and $\frac{h}{2} - t_f \leq z_N \leq \frac{h}{2}$.

In the range $0 \leq z_N \leq \frac{h}{2} - t_f$, the normal stress acting in the range $0 \leq z \leq z_N$ is given by Equation (20). It follows that the axial force $N(z_N)$ is given by:

$$N(z_N) = 2t_w \int_0^{z_N} \sqrt{\sigma_0^2 - 3\frac{T^2\left\{bt_f\left(h - t_f\right) + t_w\left[\left(\frac{h}{2} - t_f\right)^2 - z^2\right]\right\}^2}{4I_y^2 t_w^2}}\,dz \tag{30}$$

and the bending moment $M(z_N)$ is given by:

$$\begin{aligned} M(z_N) = 4\int_{\frac{t_w}{2}}^{\frac{b}{2}} \left[\int_{\frac{h}{2}-t_f}^{\frac{h}{2}} \sqrt{\sigma_0^2 - 3\frac{T^2}{4I_y^2}\left[\left(\frac{b}{2} - y\right)^2\left(h - t_f\right)^2 + \left(\frac{h^2}{4} - z^2\right)^2\right]}\,z\,dz\right] dy \\ +2t_w \int_{\frac{h}{2}-t_f}^{\frac{h}{2}} \sqrt{\sigma_0^2 - 3\frac{T^2\left(\frac{h^2}{4} - z^2\right)^2}{4I_y^2}}\,z\,dz \\ +2t_w \int_{z_N}^{\frac{h}{2}-t_f} \sqrt{\sigma_0^2 - 3\frac{T^2\left\{bt_f\left(h - t_f\right) + t_w\left[\left(\frac{h}{2} - t_f\right)^2 - z^2\right]\right\}^2}{4I_y^2 t_w^2}}\,z\,dz \end{aligned} \tag{31}$$

In the range $\frac{h}{2} - t_f \leq z_N \leq \frac{h}{2}$, the axial force $N(z_N)$ is given by:

$$\begin{aligned} N(z_N) = 2t_w \int_0^{\frac{h}{2}-t_f} \sqrt{\sigma_0^2 - 3\frac{T^2\left\{bt_f\left(h - t_f\right) + t_w\left[\left(\frac{h}{2} - t_f\right)^2 - z^2\right]\right\}^2}{4I_y^2 t_w^2}}\,dz + \\ 4\int_{\frac{t_w}{2}}^{\frac{b}{2}} \left[\int_{\frac{h}{2}-t_f}^{z_N} \sqrt{\sigma_0^2 - 3\frac{T^2}{4I_y^2}\left[\left(\frac{b}{2} - y\right)^2\left(h - t_f\right)^2 + \left(\frac{h^2}{4} - z^2\right)^2\right]}\,dz\right] dy + 2t_w \int_{\frac{h}{2}-t_f}^{z_N} \sqrt{\sigma_0^2 - 3\frac{T^2\left(\frac{h^2}{4} - z^2\right)^2}{4I_y^2}}\,dz \end{aligned} \tag{32}$$

The bending moment $M(z_N)$ is given by:

$$M(z_N) = 4\int_{\frac{t_w}{2}}^{\frac{b}{2}}\left[\int_{z_N}^{\frac{h}{2}}\sqrt{\sigma_0^2 - 3\frac{T^2}{4I_y^2}\left[\left(\frac{b}{2}-y\right)^2\left(h-t_f\right)^2 + \left(\frac{h^2}{4}-z^2\right)^2\right]}zdz\right]dy + 2t_w\int_{z_N}^{\frac{h}{2}}\sqrt{\sigma_0^2 - 3\frac{T^2\left(\frac{h^2}{4}-z^2\right)^2}{4I_y^2}}zdz \tag{33}$$

In the range $T_E \le T \le T_p$, for $0 \le \overline{z} \le \frac{h}{2} - t_f$ the shear force is given by

$$T(\overline{z}) = \frac{\sigma_0}{\sqrt{3}}2t_w\left(\overline{z} + \int_{\overline{z}}^{\frac{h}{2}-t_f}\frac{S_y(z)}{S_y(\overline{z})}dz + \int_{\frac{h}{2}-t_f}^{\frac{h}{2}}\frac{S_y(z)}{S_y(\overline{z})}dz\right) \tag{34}$$

Once the shear force is given, the corresponding N, M domain boundary is obtained as described in the foregoing sections. By selecting different values of z_N in the range of $\overline{z} \le z_N \le \frac{h}{2}$ and identifying the portion of the web where the yield condition is reached due to the presence of normal stresses due to the axial force and shear stresses, the relevant pairs of axial force and bending moment defining the searched boundary can be obtained by considering the two subranges $\overline{z} \le z_N \le \frac{h}{2} - t_f$ and $\frac{h}{2} - t_f \le z_N \le \frac{h}{2}$ separately.

In the range $\overline{z} \le z_N \le \frac{h}{2} - t_f$, the axial force $N[T(\overline{z}), z_N]$ and the bending moment $M[T(\overline{z}), z_N]$ are given by:

$$N[T(\overline{z}), z_N] = 2t_w\int_{\overline{z}}^{z_N}\sqrt{\sigma_0^2 - 3\frac{T^2(\overline{z})\left\{bt_f\left(h-t_f\right) + t_w\left[\left(\frac{h}{2}-t_f\right)^2 - z^2\right]\right\}^2}{4I_y^2t_w^2}}dz \tag{35}$$

$$M[T(\overline{z}), z_N] = 4\int_{\frac{t_w}{2}}^{\frac{b}{2}}\left[\int_{\frac{h}{2}-t_f}^{\frac{h}{2}}\sqrt{\sigma_0^2 - 3\frac{T^2(\overline{z})}{4I_y^2}\left[\left(\frac{b}{2}-y\right)^2\left(h-t_f\right)^2 + \left(\frac{h^2}{4}-z^2\right)^2\right]}zdz\right]dy + 2t_w\int_{\frac{h}{2}-t_f}^{\frac{h}{2}}\sqrt{\sigma_0^2 - 3\frac{T^2(\overline{z})\left(\frac{h^2}{4}-z^2\right)^2}{4I_y^2}}zdz + 2t_w\int_{z_N}^{\frac{h}{2}-t_f}\sqrt{\sigma_0^2 - 3\frac{T^2(\overline{z})\left\{bt_f\left(h-t_f\right) + t_w\left[\left(\frac{h}{2}-t_f\right)^2 - z^2\right]\right\}^2}{4I_y^2t_w^2}}zdz \tag{36}$$

In the range $\frac{h}{2} - t_f \le z_N \le \frac{h}{2}$, the axial force $N[T(\overline{z}), z_N]$ and the bending moment $M[T(\overline{z}), z_N]$ are given by:

$$N[T(\bar{z}), z_N] = 4 \int_{\frac{t_w}{2}}^{\frac{b}{2}} \left[\int_{\frac{h}{2}-t_f}^{z_N} \sqrt{\sigma_0^2 - 3\frac{T^2(\bar{z})}{4I_y^2}\left[\left(\frac{b}{2}-y\right)^2\left(h-t_f\right)^2 + \left(\frac{h^2}{4}-z^2\right)^2\right]}\, dz \right] dy$$
$$+2t_w \int_{\frac{h}{2}-t_f}^{z_N} \sqrt{\sigma_0^2 - 3\frac{T^2(\bar{z})\left(\frac{h^2}{4}-z^2\right)^2}{4I_y^2}}\, dz \tag{37}$$
$$+2t_w \int_{\bar{z}}^{\frac{h}{2}-t_f} \sqrt{\sigma_0^2 - 3\frac{T^2(\bar{z})\left\{bt_f\left(h-t_f\right) + t_w\left[\left(\frac{h}{2}-t_f\right)^2 - z^2\right]\right\}^2}{4I_y^2 t_w^2}}\, dz$$

$$M[T(\bar{z}), z_N] = 4 \int_{\frac{t_w}{2}}^{\frac{b}{2}} \left[\int_{z_N}^{\frac{h}{2}} \sqrt{\sigma_0^2 - 3\frac{T^2(\bar{z})}{4I_y^2}\left[\left(\frac{b}{2}-y\right)^2\left(h-t_f\right)^2 + \left(\frac{h^2}{4}-z^2\right)^2\right]}\, z dz \right] dy$$
$$+2t_w \int_{z_N}^{\frac{h}{2}} \sqrt{\sigma_0^2 - 3\frac{T^2(\bar{z})\left(\frac{h^2}{4}-z^2\right)^2}{4I_y^2}}\, z dz \tag{38}$$

3. Numerical Application

In order to test the reliability of the domain formulations defined in the foregoing section, in the following section, numerical applications to two welded sections are presented and compared with the domain defined in the EC3 standard. The selected sections possess the geometrical characteristics reported in Table 1. As can be easily observed, with the aim of performing the necessary comparison, the geometry of section W1 is chosen with width, depth, and thickness equal to those of HEA300, while the geometry of section W2 is chosen with width, depth, and thickness equal to those of IPE360.

Table 1. Geometrical characteristics of the welded sections under examination.

Section	Width b (mm)	Depth h (mm)	Web Thickness t_w (mm)	Flange Thickness t_f (mm)
W1	300	290	8.5	14
W2	170	360	8	12.7

The equations defining the proposed domains were written in Mathematica® 14.0 software to obtain the corresponding graphs. For the plain domains, the investigated range for z was divided into 20 intervals, leading to satisfactory results, which are reported in the following section. For 3D domains, the investigated range for T was divided into 10 intervals, and for each of these intervals, 100 points were calculated. The overall computing time for each section was equal to 5 min on HP I7-32 GB RAM workstation.

As the first application, the case of the W1 section was considered. In Figure 4, the N, M domain obtained by Equations (13) and (14), the N, T domain obtained by Equations (21) and (27), and the M, T domain obtained by Equations (28) and (29) are sketched, respectively.

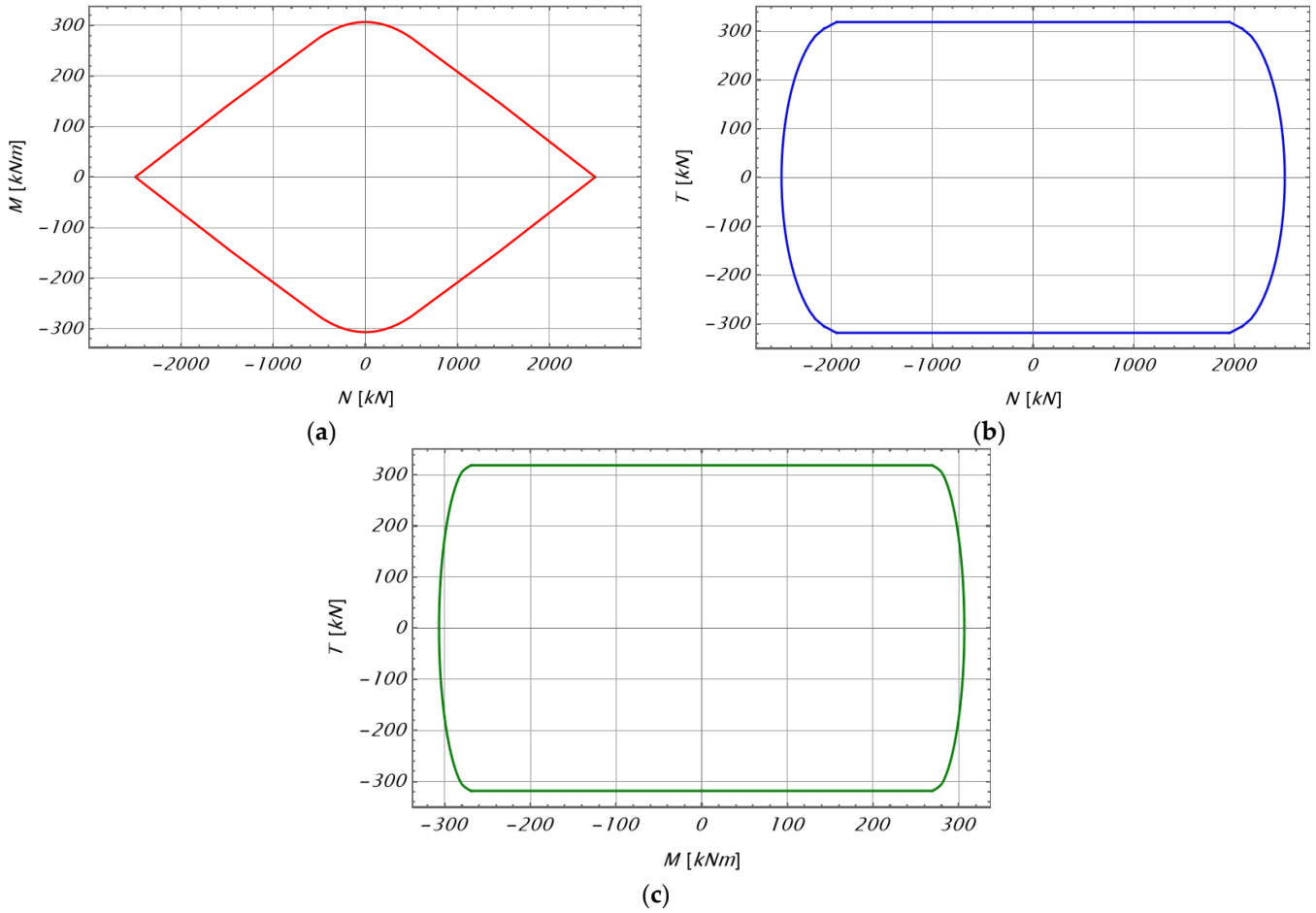

Figure 4. Yield domains for W1 section: (**a**) N, M domain; (**b**) N, T domain; (**c**) M, T domain.

In Figure 5, the N, T, M domain is sketched both with and without a bounding surface.

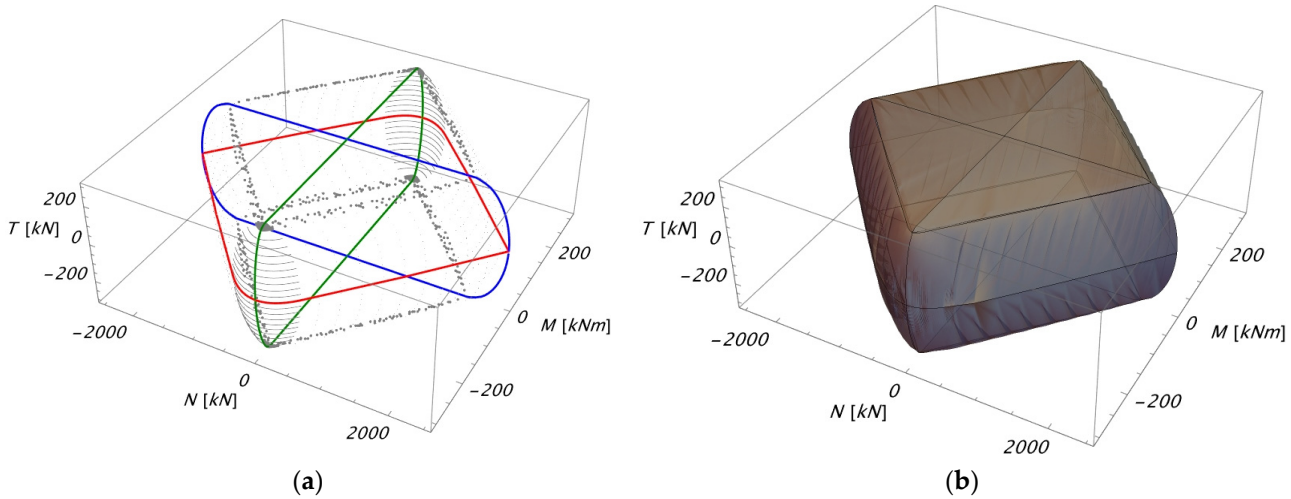

Figure 5. Proposed yield domain in N, M, T space for section W1: (**a**) 3D domain with plane domains evidenced; (**b**) 3D domain with bounding surface.

In Figure 5a, the plane domains reported in Figure 4 are also reported to enhance the overall coherence of the proposed approach.

It is worth noting that the boundary of the upper plateau of the domain in Figure 5b represents the yield conditions for the whole cross-section, while all the points within the

relevant boundary define the limit conditions related to the shear forces; in other words, for this plane domain, just the web of the cross sections is fully plasticized, while the flanges remain in the elastic regime. On the contrary, all the points of the lateral surface represent yield conditions for the whole cross-section.

To check the affordability of the proposed approach, the plane domains reported in Figure 4 are compared with those arising from the EC3 international standard and sketched in Figure 6. It is important to emphasize that the EC3 code does not provide any information about the interaction between axial and shear force. Two outcomes can be inferred from the last remark: the first is that no comparison can be made for the N, T domain sketched in Figure 4b; the second is that no limit condition is derived from the EC3 for the N, T domain, and, consequently, the 3D N, T, M is that reported in Figure 7. An examination of Figures 5–7 allows us to draw the following conclusions: the proposed domains are fully coherent with those proposed by the international standards, but they represent a rigorous definition of the real yield conditions of the cross-section subjected to the presence of axial force, shear, and bending moment; furthermore, the proposed approach can easily be extended to the case of cross-sections subjected to more complex combinations of internal forces ($N, T_y, T_z, M_x, M_y, M_z$), but this point will be considered in future studies.

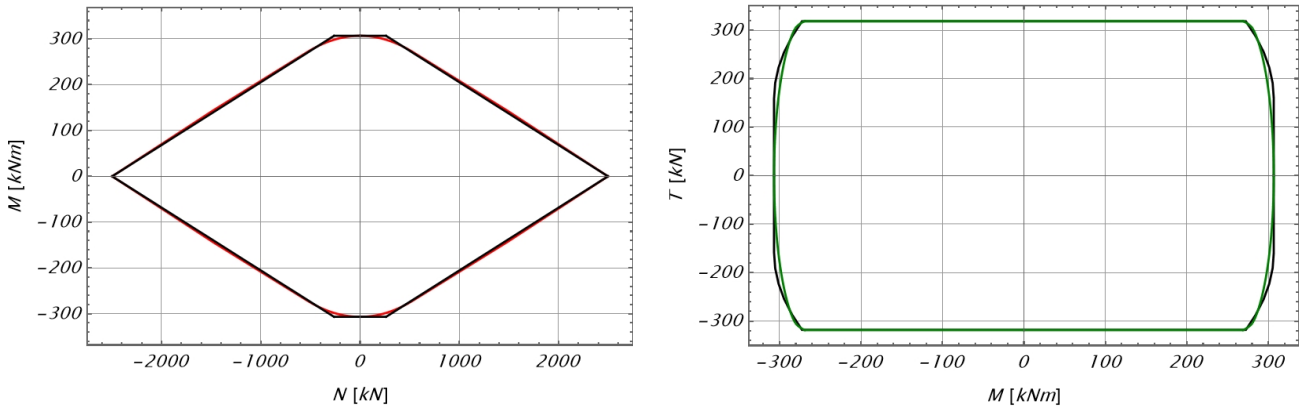

Figure 6. Comparison between the proposed plane domains and those obtained by EC3 for W1 section: (**a**) N, M domain: (black) EC3, (red) proposed one; (**b**) M, T domain: (black) EC3, (green) proposed one.

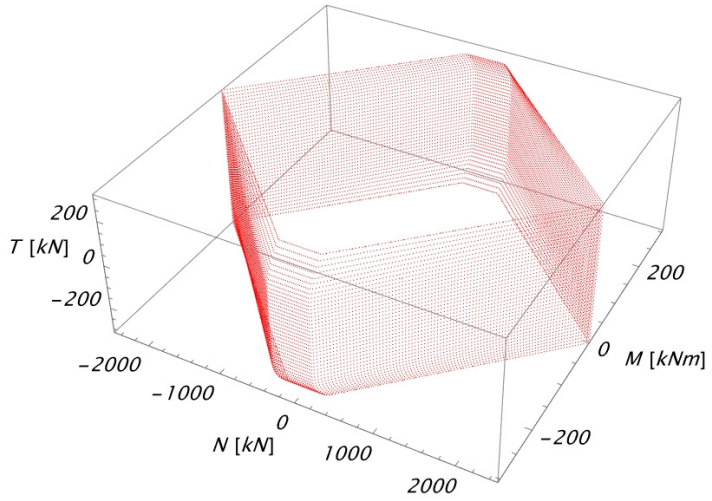

Figure 7. EC3 domain in N, M, T space for W1 section.

As a second application, the case of the W2 section is considered. In Figure 8, the N, M domain obtained by Equations (13) and (14), the N, T domain obtained by Equations (21) and (27), and the M, T domain obtained by Equations (28) and (29) are sketched, respectively.

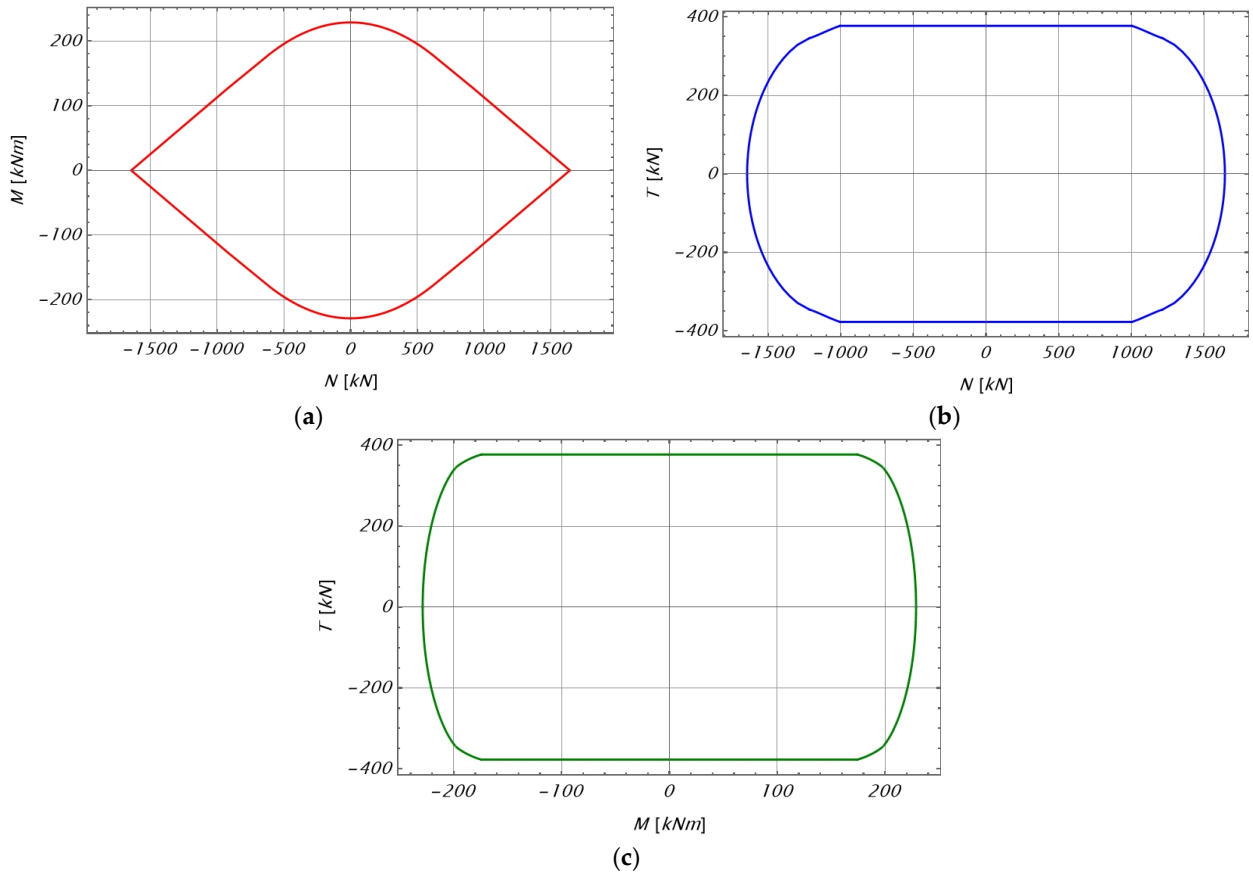

Figure 8. Plane domains for W2 section: (**a**) N, M domain; (**b**) N, T domain; (**c**) M, T domain.

In Figure 9, the N, T, M domain is sketched both with and without a bounding surface. In Figure 9a, the plane domains reported in Figure 8 are also reported to enhance the overall coherence of the proposed approach.

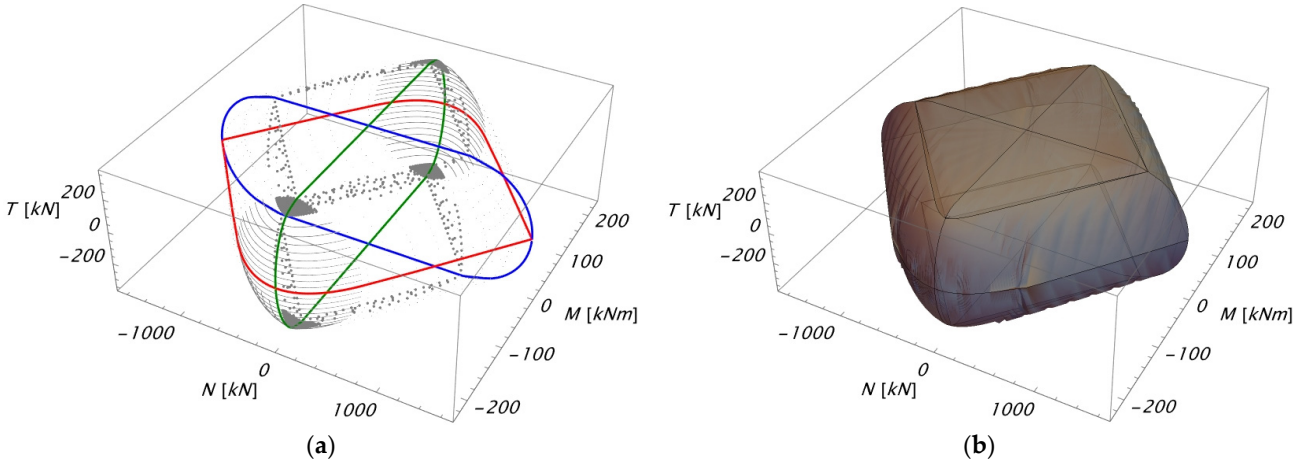

Figure 9. Proposed domain in N, M, T space for section W1: (**a**) 3D domain with plane domains evidenced; (**b**) 3D domain with bounding surface.

As previously stated, the boundary of the upper plateau of the domain in Figure 9b represents yield conditions for the whole cross-section, while all the points within the relevant boundary define limit conditions related to the shear forces, and all the points of the lateral surface represent yield conditions for the whole cross-section.

To check the affordability of the proposed approach, the plane domains reported in Figure 8 are compared with those arising from the EC3 international standard and sketched in Figure 10. As previously stated, the EC3 code does not provide any information about the interaction between axial and shear force, so no comparison can be made for the N, T domain sketched in Figure 8b, and, consequently, the 3D N, T, M related to EC3 is reported in Figure 11. The examination of Figures 9–11 allows us to make analogous remarks, as previously stated with reference to Figures 5–7.

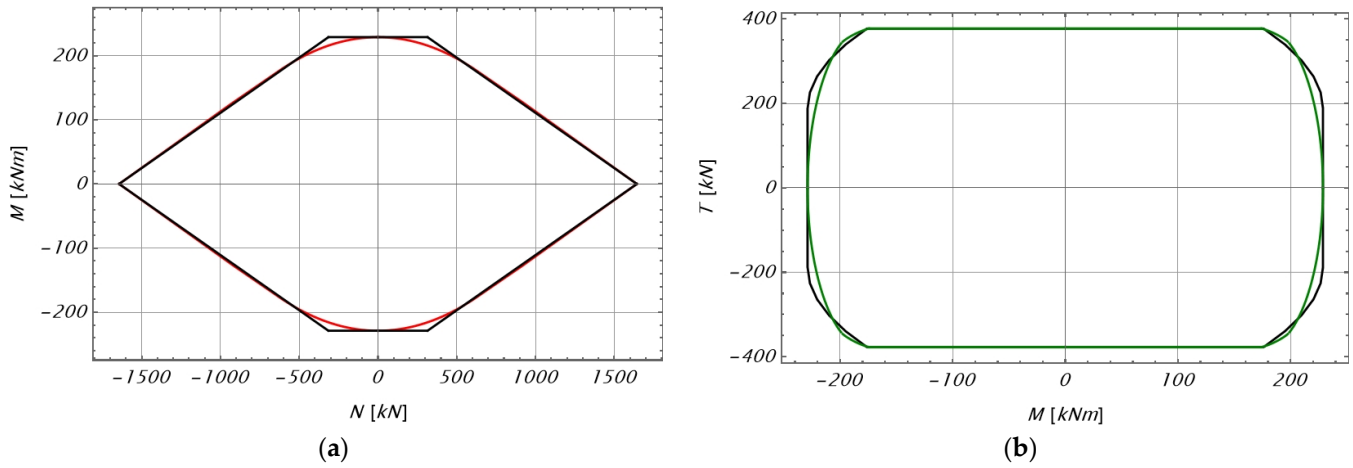

Figure 10. Comparison between the proposed plane domains and those obtained by EC3 for W2 section: (**a**) N, M domain: (black) EC3, (red) proposed one; (**b**) M, T domain: (black) EC3, (green) proposed one.

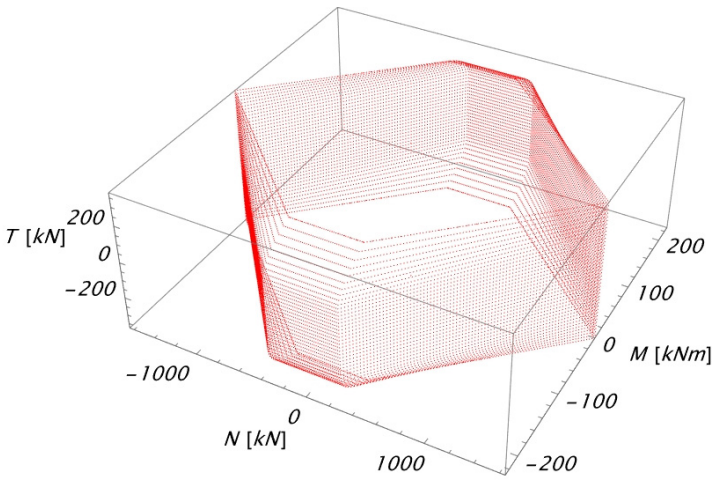

Figure 11. EC3 domain in N, M, T space for W2 section.

4. Conclusions

The proposed approach for the identification of the yield domains of I-shaped welded steel sections is rigorous and takes full advantage of the well-known classical formulas usually adopted in beam theory. The comparison with the corresponding domains obtained in agreement with the EC3 standard confirms the affordability of the proposed approach, and it allows the fact that EC3 does not propose the formulation related to the determination of the yield domain for the interaction between axial and shear forces to be overcome. The proposed approach can therefore be adopted for the analysis of I-shaped welded cross-

sections of any geometry, allowing for a more reliable design. Possible developments of the proposed study are represented by an extension to the case of the presence of different combinations of internal forces and by the specialization of the approach to the case of rolled sections, as well as to the case of welded cross-sections of any geometry. Moreover, due to the necessary manufacturing production of the welded cross-section beam elements, further in-depth analyses must be performed, consisting of appropriate experimental tests and the related FE computations. All these detailed topics will be the subjects of future papers.

Author Contributions: Conceptualization, S.B. and L.P.; validation, S.B. and L.P.; writing—original draft preparation, L.P.; writing—review and editing, S.B. and L.P. All authors have read and agreed to the published version of the manuscript.

Funding: This research received no external funding.

Institutional Review Board Statement: Not applicable.

Informed Consent Statement: Not applicable.

Data Availability Statement: Data are contained within the article.

Conflicts of Interest: The authors declare no conflicts of interest.

Appendix A

Referring to Figure A1,

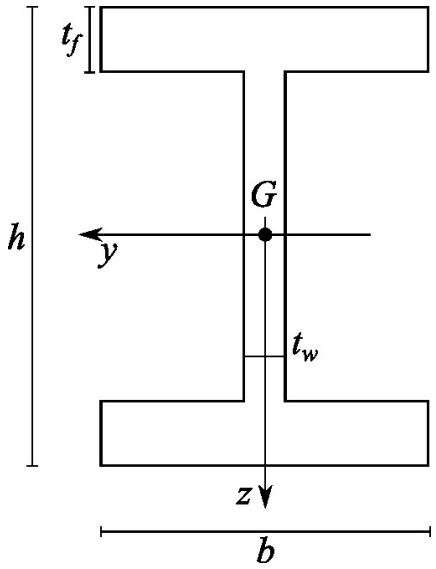

Figure A1. Geometrical sketch of the cross-section.

The following geometrical properties of the cross-section can be easily determined:

$$A = 2bt_f + t_w\left(h - 2t_f\right) = bh - (b - t_w)\left(h - 2t_f\right) \tag{A1}$$

$$I_y = b\frac{t_f^3}{6} + bt_f\frac{\left(h - t_f\right)^2}{2} + t_w\frac{\left(h - 2t_f\right)^3}{12} = \frac{bh^3}{12} - \frac{(b - t_w)\left(h - 2t_f\right)^3}{12} \tag{A2}$$

$$W_{Ey} = \frac{2I_y}{h} \tag{A3}$$

$$W_{py} = bt_f\left(h - t_f\right) + t_w\frac{\left(h - 2t_f\right)^2}{4} = \frac{bh^2}{4} - \frac{(b - t_w)\left(h - 2t_f\right)^2}{4} \tag{A4}$$

A, I_y, W_{Ey} and W_{Py} represent the area, the second-order moment of area (with respect to the y-axis), the elastic modulus (with respect to the y-axis) and the plastic modulus (with respect to the y-axis), of the given section, respectively.

Finally, the first-order moment of area of the portion of the area of the given section below the y-axis evaluated with respect to the y-axis, is given by:

$$S_{y,G} = bt_f\left(\frac{h-t_f}{2}\right) + \frac{t_w}{2}\left(\frac{h}{2}-t_f\right)^2 = \frac{bh^2}{8} - \frac{(b-t_w)\left(\frac{h}{2}-t_f\right)^2}{2} \quad \text{(A5)}$$

References

1. Gokhfeld, D.A.; Cherniavsky, D.F. *Limit Analysis of Structures at Thermal Cycling*; Springer: Dordrecht, The Netherland, 1980; ISBN 978-90-286-0455-1.
2. Marti, K. Limit load and shakedown analysis of plastic structures under stochastic uncertainty. *Com. Meth. App. Mech. Eng.* **2008**, *198*, 42–51. [CrossRef]
3. Palizzolo, L.; Benfratello, S.; Tabbuso, P.; Vazzano, S. Reliable measures of plastic deformations for elastic plastic structures in shakedown conditions. In Proceedings of the 24th Conference of the Italian Association of Theoretical and Applied Mechanics, AIMETA 2019, Rome, Italy, 15–19 September 2019; ISBN 978-303041056-8. [CrossRef]
4. Chen, W.; Duan, L. *Plasticity, Limit Analysis, Stability and Structural Design: An Academic Life Journey from Theory to Practice*; World Scientific: Singapore, 2021; ISBN 978-981122974-9/978-981122973-2.
5. Huang, M.F.; Li, Q.; Chan, C.M.; Lou, W.J.; Kwok, K.C.S.; Li, G. Performance-based design optimization of tall concrete framed structures subject to wind excitations. *J. Wind. Eng. Ind. Aerodyn.* **2015**, *139*, 70–81. [CrossRef]
6. Tabbuso, P.; Spence, S.M.J.; Palizzolo, L.; Pirrotta, A.; Kareem, A. An efficient framework for the elasto-plastic reliability assessment of uncertain wind excited systems. *Struct. Saf.* **2016**, *58*, 69–78. [CrossRef]
7. Benfratello, S.; Di Paola, M.; Palizzolo, L.; Tabbuso, P. Evaluation of the shakedown limit load multiplier for stochastic seismic actions. *Meccanica* **2017**, *52*, 2735–2750. [CrossRef]
8. Zhang, R.; Wang, W.; Alam, M.S. Seismic evaluation of friction spring-based self-centering braced frames based on life-cycle cost. *Earthq. Eng. Struct. Dyn.* **2022**, *51*, 3393–3415. [CrossRef]
9. Hu, S.; Zhu, S. Life-cycle benefits estimation for hybrid seismic-resistant self-centering braced frames. *Earthq. Eng. Struct. Dyn.* **2023**, *52*, 3097–3119. [CrossRef]
10. Banichuk, N.V. *Introduction to Optimization of Structures*; Springer: New York, NY, USA, 1990; ISBN 978-1-4612-7988-4. [CrossRef]
11. Se-Hyu, C.; Seung-Eock, K. Optimal design of steel frame using practical nonlinear inelastic analysis. *Eng. Struct.* **2002**, *24*, 1189–1201. [CrossRef]
12. Degertekin, S.O. Improved harmony search algorithms for sizing optimization of truss structures. *Comp. Struct.* **2012**, *92–93*, 229–241. [CrossRef]
13. Benfratello, S.; Giambanco, F.; Palizzolo, L.; Tabbuso, P. Structural design of frames able to prevent element buckling. In Proceedings of the 11th International Conference on Computational Structures Technology, CST 2012, Civil-Comp Proceedings, Dubrovnik, Croatia, 4–7 September 2012; Volume 99, ISBN 978-190508854-6.
14. Benfratello, S.; Giambanco, F.; Palizzolo, L.; Tabbuso, P. Optimal design of steel frames accounting for buckling. *Meccanica* **2013**, *48*, 2281–2298. [CrossRef]
15. Palizzolo, L.; Caffarelli, A.; Tabbuso, P. Minimum volume design of structures with constraints on ductility and stability. *Eng. Struct.* **2014**, *68*, 47–56. [CrossRef]
16. Palizzolo, L.; Benfratello, S.; Tabbuso, P. Discrete variable design of frames subjected to seismic actions accounting for element slenderness. *Comput. Struct.* **2015**, *147*, 147–158. [CrossRef]
17. Kaveh, H.; Nasrollahi, A. Performed-based seismic design of steel frames utilizing charged system search optimization. *Appl. Soft Comput.* **2014**, *22*, 213–221. [CrossRef]
18. Benfratello, S.; Palizzolo, L.; Tabbuso, P. Optimal design of elastic plastic frames accounting for seismic protection devices. *Struct. Multidiscip. Optim.* **2014**, *49*, 93–106. [CrossRef]
19. Zhang, R.; Hu, S. Optimal design of self-centering braced frames with limited self-centering braces. *J. Build. Eng.* **2024**, *88*, 109201. [CrossRef]
20. Benfratello, S.; Palizzolo, L.; Tabbuso, P. Optimization of structures with unrestricted dynamic shakedown constraints. *Struct. Multidiscip. Optim.* **2015**, *52*, 431–445. [CrossRef]
21. Colajanni, P.; La Mendola, L.; Monaco, A.; Pagnotta, S. Seismic Performance of Earthquake-Resilient RC Frames Made with HSTC Beams and Friction Damper Devices. *J. Earth. Eng.* **2022**, *26*, 7787–7813. [CrossRef]
22. Colajanni, P.; La Mendola, L.; Monaco, A.; Pagnotta, S. Design of RC joints equipped with hybrid trussed beams and friction dampers. *Eng. Struct.* **2021**, *227*, 111442. [CrossRef]
23. Colajanni, P.; Pagnotta, S. Friction-based beam-to-column connection for low-damage RC frames with hybrid trussed beams. *Struct. Eng. Mech.* **2022**, *45*, 231–248. [CrossRef]

24. Plumier, A.; Doneux, C.; Castiglioni, C.; Brescianini, J.; Crespi, A.; Dell' Anna, S.; Lazzarotto, L.; Calado, L.; Ferreira, J.; Feligioni, S.; et al. *Two Innovations for Earthquake Resistant Design—The INERD Project—Final Report*; Research Programme of the Research Fund for Coal and Steel. Steel RTD, Report EUR22044EN; 2006; ISBN 92-79-01694-6. Available online: https://op.europa.eu/en/publication-detail/-/publication/ccd50305-1c81-4eea-b937-fa05f81e2b18/language-en (accessed on 5 July 2024).
25. Iwankiw, N.R.; Carter, C.J. The dogbone: A new idea to chew on. *Mod. Steel Constr.* **1996**, *36*, 18–23.
26. Plumier, A. The dogbone: Back to the future. *Eng. J.* **1997**, *34*, 61–67. [CrossRef]
27. Engelhardt, M.D.; Winneberger, T.; Zekany, A.J.; Potyray, T.J. Experimental investigation of dogbone moment connections. *Eng. J.* **1998**, *35*, 128–139. [CrossRef]
28. Miller, D.K. Lessons learned from the Northridge earthquake. *Eng. Struc.* **1998**, *20*, 249–260. [CrossRef]
29. Mahin, S.T. Lessons from damage to steel buildings during the Northridge earthquake. *Eng. Struct.* **1998**, *20*, 261–270. [CrossRef]
30. Shen, J.; Kitjasateanphun, T.; Srivanich, W. Seismic performance of steel moment frames with reduced beam sections. *Eng. Struct.* **2000**, *22*, 968–983. [CrossRef]
31. Horton, T.A.; Hajirasouliha, I.; Davison, B.; Ozdemir, Z. More efficient design of reduced beam sections (RBS) for maximum seismic performance. *J Constr Steel Res.* **2021**, *183*, 106728. [CrossRef]
32. Shakeri, K.; Akrami, V.; Moradpour, S.; Khedmati, S. Post-earthquake Behavior of Steel Moment Resisting Frames with Connections Modified by Introducing Reduced Beam Section (RBS). *Int. J. Steel Struct.* **2024**, *24*, 462–476. [CrossRef]
33. Mirghaderi, S.R.; Shahabeddin, T.; Imanpour, A. Seismic performance of the accordion-web RBS connection. *J. Constr. Steel Res.* **2010**, *66*, 277–288. [CrossRef]
34. Saleh, A.; Mirghaderi, S.R.; Zahrai, S.M. Cyclic testing of tubular web RBS connections in deep beams. *J. Constr. Steel Res.* **2016**, *117*, 214–226. [CrossRef]
35. Momenzadeh, S.; Kazemi, M.T.; Asl, M.H. Seismic performance of reduced web section moment connections. *Int. J. Steel Struct.* **2017**, *17*, 413–425. [CrossRef]
36. Tabar, A.M.; Alonso-Rodriguez, A.; Tsavdaridis, K.D. Building retrofit with reduced web (RWS) and beam (RBS) section limited-ductility connections. *J. Constr. Steel Res.* **2022**, *197*, 107459. [CrossRef]
37. Dimakogianni, D.; Dougka, G.; Vayas, I. Seismic behavior of frames with innovative energy dissipation systems (FUSEIS1-2). *Eng. Struct.* **2015**, *90*, 83–95. [CrossRef]
38. Valente, M.; Castiglioni, C.A.; Kanyilmaz, A. Welded fuses for dissipative beam-to-column connections of composite steel frames: Numerical analyses. *J. Constr. Steel Res.* **2017**, *128*, 498–511. [CrossRef]
39. Avgerinou, S.; Thanopoulos, P.; Hoffmeister, B.; Vayas, I. Seismic resistant buildings with dissipative elements made of high strength steel [Erdbebensichere Bauten mit dissipativen Elementen aus hochfestem Stahl]. *Stahlbau* **2022**, *91*, 326–337. [CrossRef]
40. Benfratello, S.; Caddemi, S.; Palizzolo, L.; Pantò, B.; Rapicavoli, D.; Vazzano, S. Targeted steel frames by means of innovative moment resisting connections. *J. Constr. Steel Res.* **2021**, *183*, 106695. [CrossRef]
41. Benfratello, S.; Palizzolo, L. Prevention of brittle failure for steel connections utilizing special devices. *Structures* **2024**, *62*, 106153. [CrossRef]
42. Benfratello, S.; Palizzolo, L.; Vazzano, S. A New Design Problem in the Formulation of a Special Moment Resisting Connection Device for Preventing Local Buckling. *J. Appl. Sci.* **2022**, *12*, 202. [CrossRef]
43. European Committee for Standardization. *EN 1993-1-8:2006*; Eurocode 3: Design of Steel Structures Part 1–8: Design of Joints; European Committee for Standardization: Bruxelles, Belgium, 2006.
44. Goczek, J.; Supeł, Ł. Resistance of steel cross-sections subjected to bending, shear and axial forces. *Eng. Struct.* **2014**, *70*, 271–277. [CrossRef]